Evaluating aggregate stability, surface properties and disintegration behavior of bauxite residue induced by Ca/Na

by Xue, S., Ke, W., Zhu, F., Fan, J., Wang, Q., Liu, Z. and Hartley, W

Xue, S., Ke, W., Zhu, F., Fan, J., Wang, Q., Liu, Z. and Hartley, W. 2020 Evaluating aggregate stability, surface properties and disintegration behavior of bauxite residue induced by Ca/Na. *Land Degradation & Development*.
28 June 2020

Evaluating aggregate stability, surface properties and disintegration behavior of bauxite residue induced by Ca/Na

Shengguo Xue[a, b], Wenshun Ke[a], Feng Zhu[a,b*], Jiarong Fan[b], , Qiongli Wang[a], Zheng Liu[a], William Hartley[c]

[a] School of Metallurgy and Environment, Central South University, Changsha 410083, PR China

[b] Chinese National Engineering Research Center for Control and Treatment of Heavy Metal Pollution, Central South University, Changsha 410083, China

[c] Crop and Environment Sciences Department, Harper Adams University, Newport, Shropshire, TF10 8NB, United Kingdom

ABSTRACT

Bauxite residue contains large concentrations of exchangeable Na^+, which fragments aggregate structure and limits plant growth. Understanding the potential mechanisms of Ca/Na on the formation process of residue aggregates will benefit the screening of appropriate amendments for ecological reconstruction on bauxite residue disposal areas. A method for evaluating aggregate behavior and stability by integration of Le Bissonnais' and laser diffraction measurements, was determined on bauxite residues following Ca/Na additions. With increasing Ca^{2+} addition, mean weight diameter (MWD) increased, indicating improved resistance to dispersion. Ca^{2+} had a positive effect on flocculation of silt-size microaggregates, whilst disintegration was induced following Na+ addition. Repeated laser diffraction analysis of residue samples circulating in 50 mmol L-1 electrolyte solution (Ca^{2+}/Na^+) provided a detailed view of the changes in particle size distribution as aggregates fragmented. The visualized 3D surface map revealed that Na^+ promotes the disintegration of residue aggregates into finer dispersed particles, whilst Ca^{2+} protects the microaggregates from fragmenting into smaller particles. Variation in electrochemical properties of aggregate surfaces affected the micro-morphology significantly. The findings provide a new approach to specify pedogenic aggregate behavior of bauxite residue, whilst revealing the effects of Ca^{2+}/Na^+ on aggregate stability, surface electrochemical properties and its micromorphology. This new approach will be beneficial to the assessment of soil formation and ecological reconstruction on bauxite residue disposal areas.

HIGHLIGHTS

1. Aggregate behavior and stability of bauxite residue induced by Ca/Na are evaluated.
2. Integration of Le Bissonnais' and laser diffraction methods may effectively reveal aggregate fragmentation.
3. Ca/Na addition transformed surface electrochemical properties and micro-morphology of residue aggregates.
4. Ca^{2+} stimulated aggregate formation, whilst Na^+ resulted in particles dispersion.

* Corresponding author.
E-mail address: zhufeng1990@csu.edu.cn (Feng Zhu); sgxue70@hotmail.com (Shengguo Xue)

Keywords

Bauxite residue, aggregate stability, laser diffraction, surface electrochemistry, soil formation

1. Introduction

Bauxite residue, a highly alkaline solid waste, is produced by alumina extraction from bauxite ore by the Bayer process (Santini et al., 2015; Kong et al., 2017). Globally, the inventory of bauxite residue has reached 4.6 Gt, and increased at a rate of 200 Mt per annum (Xue et al., 2019). Disposing and storing these large volumes of residue still remains an increasing environmental risk (Burke et al., 2013). Ecological reconstruction is a promising way forward for the remediation of bauxite residue on a large scale, reducing environmental risks (Xue et al., 2016). Nevertheless, bauxite residue has high salinity (electrical conductivity≈7.4 mS cm^{-1}) and alkalinity (pH≈11.3, exchangeable sodium percentage≈69 %), and a fine particle composition (Grafe et al., 2012); these properties result in poor aggregate structure and water holding capacity, which limit plant survival (You et al., 2019).

During the last few decades, a number of studies have focused on the removal of alkalinity and salinity in the residues prior to field rehabilitation. However, it has been increasingly recognized that for successful cover establishment on mine residues, the processes of soil development is critical. Soil aggregates are the basic unit of soil structure and aggregate stability affects the exchange of water, nutrients, gases and heat in soil, as well as the growth and metabolism of animals and microorganisms (Papadopoulos et al., 2009; Tang et al., 2011; Yang et al., 2019). Various methods including wet sieving and Le Bissonnais' (LB's) method have been proposed to characterize aggregate formation due to the complexity of mechanisms on particle aggregation or disintegration (Barthès and Roose, 2002; Almajmaie et al., 2016). Amongst them, Le Bissonnais' method (LB) can simulate different wetting conditions and energies to identify different disaggregation mechanisms. These stability tests do not exhibit the rate of aggregate slaking and the disintegration behavior of the intermediate stages, which may be critical to understanding the response of aggregates to rainfall or other destructive processes. Field et al. (2006) used a combined method of ultrasonication and sieving to destroy soil aggregates and found that aggregate disintegration may be modeled as a first-order reaction to represent aggregate behavior. Kasmerchak et al. (2018) applied repetitive laser diffraction measurements on soil samples to characterize aggregate stability and assess the effects of organic carbon and other chemical properties on soil aggregate behavior. The circulation time of 180 minutes was appropriate to monitor aggregate decomposition following laser diffraction measurement (Mason et al., 2011).

Dispersion or flocculation of aggregates was related to pH, electrolyte and exchangeable base concentrations (Shainberg and Singer, 2011). Curtin et al. (1995) found that Na addition caused clay expansion and disintegration of unstable aggregates. Le Bissonnais et al. (Le bissonnais, 1996a) observed that the cation hydration radius and valence states were important factors which affected aggregate stability; multivalent cations had a strong flocculation effect, whilst monovalent cations had a strong dispersion effect. Furthermore, the interaction force between soil particles was the intrinsic driving force for agglomerate fragmentation (Li et al., 2013). Compared to the various external forces in the erosion theory, the internal forces, including electrostatic repulsion between soil particles, were more able to determine soil disaggregation (Hu et al., 2015). According to the DLVO theory of colloidal particle interaction, electrostatic repulsion was controlled by the electric field around the particle, and electric field intensity was determined by the ion interface reaction characteristics (Santos and Yan, 2011). Salt ions in bauxite residue pore water are dominated by Na^+, K^+, Ca^{2+}, Mg^{2+}, $Al(OH)_4^-$, SO_4^{2-}, CO_3^{2-}, and

OH^- (Xu et al., 2018). The high concentrations of soluble ions and exchangeable bases may significantly affect aggregate formation and its stability.

Calcium-contained solid wastes have been applied to ameliorate physical and chemical properties of bauxite residue to support plant growth. However, understanding the potential mechanisms of Ca^{2+}/Na^+ on aggregate behavior and its stability for bauxite residue remain scarce. The hypothesis for this study was that following Ca^{2+} or Na^+ addition, surface properties and disintegration behavior varied, which changed aggregate size distribution and micro-morphology of residue aggregates. The objectives of this research were to 1) investigate aggregate size distribution and its stability using LB's method following Ca^{2+} or Na^+ addition; 2) analyze the effect of Ca^{2+} or Na^+ on variations of surface electrochemical properties of residue aggregates; 3) to quantify the disintegration rate of residue aggregates using Laser diffraction analysis.

2. Materials and methods

2.1 Materials

Fresh bauxite residue was collected to a depth of 20 cm from a bauxite residue disposal area in Central China. The climate is warm temperate continental monsoon, with an average daily temperature of 12.2-14.8 °C and mean annual precipitation of 600-700 mm. Samples were subsequently stored in polyethylene bags, returned to the laboratory, air-dried at room temperature for 2 weeks and then passed through a 2 mm sieve prior to analysis.

2.2 Aggregate disintegration

Different concentrations of NaCl and $CaCl_2$ solutions (0, 5, 10, 20, 50, 80, 100, and 200 mmol/L) were selected to determine aggregate disintegration using the modified Le Bissonnais' (LB) method (Le Bissonnais, 1996). This method included three disruptive tests: fast wetting (FW), slow wetting (SW) and wet stirring (WS). For the FW test, 6 g of 1-2mm residue aggregates were quickly immersed in NaCl or $CaCl_2$ solutions for 10 min. For SW, 6 g of 1-2mm residue aggregates were placed on filter paper upon a sponge soaked in ethanol for 30 min. For WS, 6 g of 1-2mm residue aggregates were gently immersed in ethanol for 10 min prior to immersion in NaCl or $CaCl_2$ solutions and subsequently shaken in ethanol. The aggregates were then collected by sieving (1mm, 0.25mm and 0.05mm) and the fractions in each sieve collected, dried at 40 ℃ for 24 h and weighed. Mean weight diameter (MWD) and percentage aggregate destruction (PAD) of the residue samples were calculated using the following equations:

$$MWD = \sum_{i=1}^{n} \overline{X_i} \times W_i \qquad (1)$$

$$PDA_{x/w} = \frac{W_w - W_x}{W_w} \times 100\% \qquad (2)$$

Where $\overline{X_i}$ was the mean diameter over the adjacent sieves (mm), W_i was the percentage of residue aggregates in the size range and n was the number of sample sieves. W_w was the percentage of >X mm residue aggregates after wet sieving using deionized water, and W_x was the percentage of >X mm residue aggregates after wet sieving using the electrolyte solution.

2.3 Surface electrochemical properties of residue aggregates

Bauxite residue, which was treated by different concentrations of NaCl or $CaCl_2$ solutions, was separated through a 0.05 mm sieve and the <0.05 mm fractions were dried at 40 ℃ for 24 h. The fractions were then added to a HCl solution (0.1 mol/L) (v:w=5:1), oscillated for 5 hours, centrifuged at a speed of 4000 rpm for 5 min, washed several times using deionized water to remove excess Cl^- in the suspension and separated to obtain the residues. 5 g of the residue was added into a 50 ml centrifuge tube and mixed with 10 mL $Ca(OH)_2$ and NaOH solution (0.015 mol/L). The mixtures were oscillated for 24 hours and subsequently adjusted to pH 7 using HCl. The concentrations of Ca^{2+} and Na^+ in the supernatant were then determined using ICP-MS (Hu et al., 2015).

The surface potential (φ(V)), surface electric field intensity (E), and specific surface area (S) of residue aggregates were calculated by the following equations (Li et al., 2011):

$$\varphi = \frac{2RT}{(2\beta_{Ca} - \beta_{Na})F} \ln \frac{a^0_{Ca} N_{Na}}{a^0_{Na} N_{Ca}} \quad (3)$$

$$E = \frac{4\pi}{\varepsilon}\sigma \quad (4)$$

$$S = \frac{N_{Na} k}{m a^0_{Na}} e^{\frac{F\varphi\beta_{Na}}{2RT}} = \frac{N_{Ca} k}{m a^0_{Ca}} e^{\frac{F\varphi\beta_{Ca}}{2RT}} \quad (5)$$

$$K = \sqrt{\frac{8\pi F^2 \left(\frac{1}{2}\sum a_i^0 Z_i^2\right)}{\varepsilon RT}} \quad (6)$$

$$a_i^0 = \gamma_i c_i^0 \quad (7)$$

$$\log\gamma_i = 0.512 Z_i^2 \left(\frac{I^{1/2}}{I + I^{1/2}} - 0.3I\right) \quad (8)$$

$$\beta_{Ca} = 0.0213 \ln\left(I^{0.5}\right) + 1.2331 \quad (9)$$

$$\beta_{Na} = 0.0213 \ln\left(I^{0.5}\right) + 0.7669 \quad (10)$$

$$m = 0.5259 \ln\left(c^0_{Na} / c^0_{Ca}\right) + 1.992 \quad (11)$$

Where R(J/K mol) is a universal gas constant, T(K) the system temperature, F(C/mol) the Faraday constant, k (1/dm) the Debye-Huckel constant, and ε the dielectric constant of water. I (mol/L) was the ionic strength, a^0_{Na} and a^0_{Ca} (mol/L) respectively for the activity of Na^+ and Ca^{2+} in the solution at equilibrium, N_{Na} and N_{Ca}(mol) are the adsorption capacities of Na^+ and Ca^{2+} in the residue, respectively. c^0_{Na} and c^0_{Ca} (mol/L) were concentration of Na^+ and Ca^{2+}in the solution at equilibrium. β_{Na} and β_{Ca} were correction coefficients for correcting the effective charge amount of Na^+ and Ca^{2+}, respectively.

2.4 Analysis of aggregate behavior

In order to investigate the effect of Ca or Na on residue aggregation, residue samples which were treated by 50 mmol/L NaCl and $CaCl_2$ solutions were selected to determine aggregate behavior using a laser particle analyzer (Malvern Mastersizer 2000). The analytical method is described by Mason et al. (2011) and Kasmerchar et al. (2018) as follows: selected aggregate samples were added continuously

into a beaker containing 500ml of deionized water or 50 mmol/L $CaCl_2$/NaCl solutions until the solution obscuration reached 5%-10%. Then the particle size distributions (PSD) of residue aggregates can be measured through a laser diffraction analysis cell. The PSD was measured every two minutes for the first 20 minutes and every ten minutes for the last 160 minutes. During the 180-minute measurement period, the solution was constantly stirred at a constant speed of 2000 rpm and pumped to the laser diffraction analysis cell. According to the methodology of Mason et al. (Mason et al., 2011), variations of >250 μm and <20 μm fractions were determined and fitted using the following equations:

$$\%>250\mu\mathrm{m}=\mathrm{A_1}\times\exp\left(-\mathrm{K_1T}\right)+\mathrm{C1} \quad (12)$$

$$\%<20\ \mu\mathrm{m}\ =\ \mathrm{A_2}*\left[1-\exp\left(-\mathrm{K_2T}\right)\right]+\mathrm{C2} \quad (13)$$

where K_1 and K_2 are rate constants, T is circulation time, A_1 and A_2 are rate coefficients, C_1 is the final percentage of >250 μm fractions, and C_2 represents the initial percentage of <20 μm fractions in the residue aggregates. The parameters A_1, A_2, k_1, k_2, C_1 and C_2 were determined using the obtained PSD data to fit Eqs. (15-16) and minimize the quadratic sum of residuals from models (Field and Minasny, 1999).

2.5 Morphological analysis

SEM-EDS of <0.05 mm residue aggregates from the three different treatments (DI, and 50 mmol/L NaCl/$CaCl_2$) were scanned using a scanning electron microscope (ESEM, Quanta-200). The samples were sprayed with Au prior to scanning using a GSED field emission gun.

2.6 Statistical methods

All data were analyzed in Excel 2010, IBM® SPSS® Statistics version.21, OriginLab® Origin® r. 9.0. and MATLAB R2017b. All figures and lines representing first-order models were constructed by Origin 9.0. The three-dimensional surface map of the particle size distribution of bauxite residue aggregates after different ion treatments was draw by MATLAB R2017b.

3. Results and discussion

3.1 Effect of Ca^{2+}/Na^+ on aggregate size distribution

Aggregate size distribution of bauxite residue following different treatments is presented in Fig. 1. For the FW test (simulating the slaking process), <0.05 mm aggregates were the major fraction. With $CaCl_2$ treatment, the proportion of 2-0.25 mm aggregates ranged from 45.92% to 52.02%, which were higher than in untreated residues. With increasing Na^+ concentration, the proportion of <0.05 mm microaggregates increased from 42.5% to 54.4%. For the SW test (simulating differential clay swelling processes) and the WS test (simulating the mechanism of breakdown processes), 2-1 mm aggregates were the major fractions. With $CaCl_2$ treatment, the proportions of 2-1 mm aggregates increased from 60.9% to 62.2% and 69.8% for the SW and WS test, respectively.

Ca^{2+} and Na^+ are the critical cations in bauxite residue (Xue et al., 2019), and their concentrations can significantly affect aggregation processes. Aggregate size distribution from the modified LB method revealed that Ca may increase the proportion of water-stable aggregates (>0.25 mm), whilst Na^+ resulted

in disaggregation of larger sized aggregates.

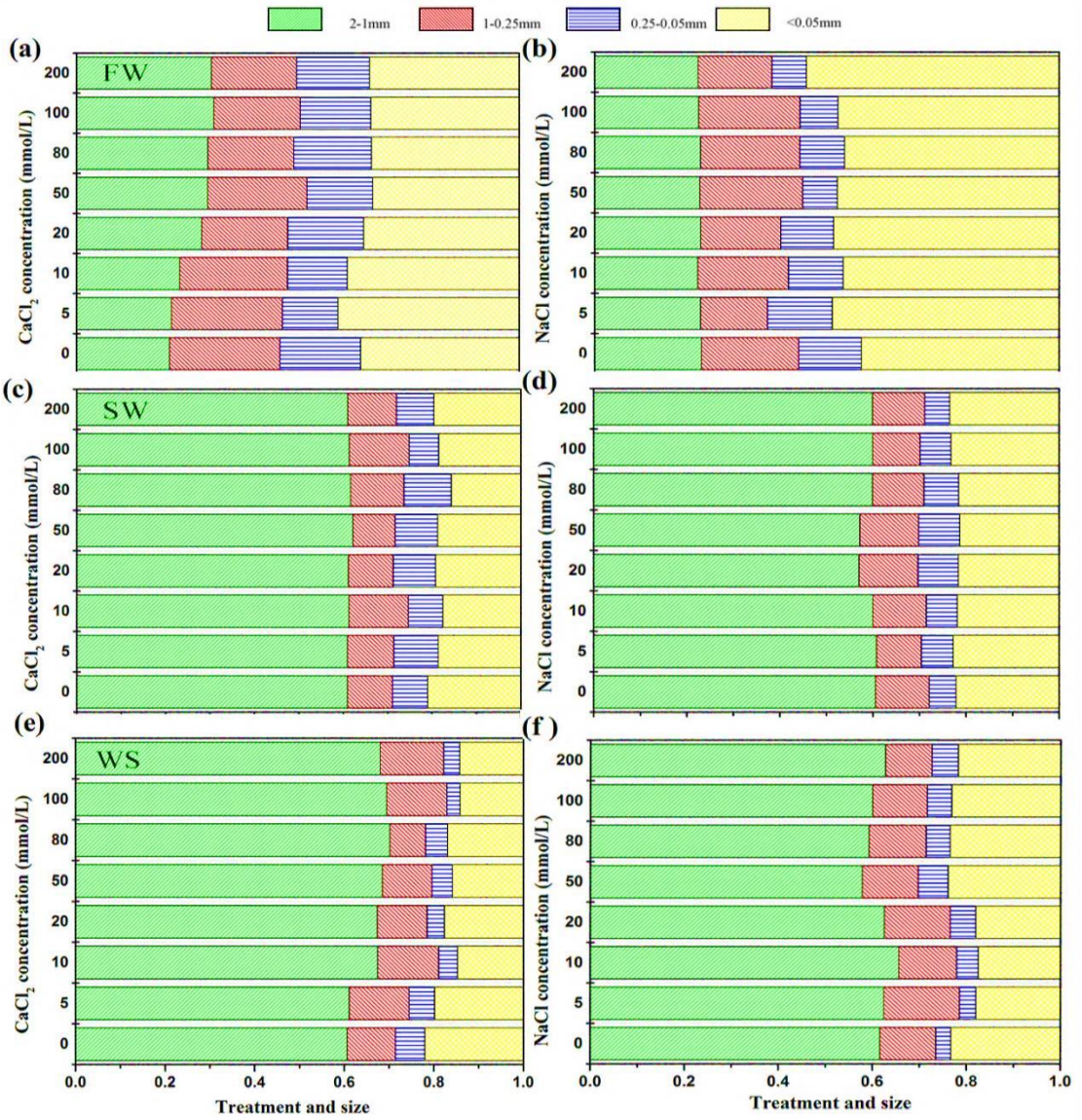

Fig. 1 Effect of Ca^{2+}/Na^{+} on aggregate fraction distribution of the treated residues from the modified Le Bissonnais' method: a & b) FW test; c & d) SW test; e & f) WS test.

MWD is a characteristic indicator used to evaluate aggregate stability and a large MWD indicates improved aggregate stability (Mbagwu and Auerswald, 1999; You et al., 2018; Cui et al., 2019). Variation in MWD following NaCl and $CaCl_2$ additions are presented in Fig. 2. For the three different tests, $CaCl_2$ addition increased MWD due to the accumulation of larger sized fractions. With increasing NaCl concentration, MWD decreased, although this did fluctuate. When the electrolyte concentration was 50 mmol/L, MWD of $CaCl_2$ treated samples reached a relatively high value, whilst a relatively low value occurred for NaCl treatments.

Electrolyte concentration, and cation valence state, significantly affected the formation of stable aggregates, especially for flocculation and dispersion of clay-size particles (Olis, 1989). Multivalent cations, including Ca^{2+}, Fe^{3+} and Al^{3+}, all formed ion bridges, compressing the thickness of the electric double layer, and promoting particle flocculation (Jiang et al., 2012). In this study, addition of $CaCl_2$

accumulated the proportion of macroaggregates (>0.25 mm), improved aggregate stability and enhanced erosion resistance of residues. The residue contained a large amount of Na^+, which resulted in particle dispersion and poor physical condition. Results demonstrated that NaCl increased the proportion of <0.05 mm microaggregates whilst reducing the stability of residue aggregates. Monovalent cations disperse aggregates whilst multivalent cations promote flocculation. Le Bissonnais (Le Bissonnais, Y., 2016.) considered that multivalent cations may effectively promote flocculation of aggregates, whilst monovalent cations have a strong dispersive effect. An excess of Na^+ may weaken covalent interaction between organic molecules and clay-sized particles, which may lead to aggregate dispersion. Zhu et al., (2017) observed that Na^+ was negatively correlated with aggregate stability in bauxite residue following amendment addition, which was consistent with the results of this study.

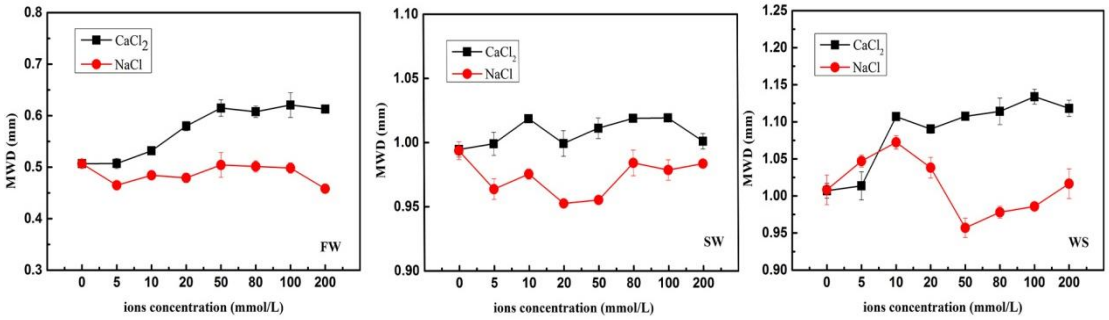

Fig.2 Effect of Ca^{2+}/Na^+ on aggregate stability of bauxite residue. a) FW test; b) SW test; c) WS test.

The percentage of aggregate destruction (PADx), which is the fraction of >x mm aggregates after wet sieving, may be used to evaluate variation in water-stable aggregates (GUBER et al., 2005). A positive value for PADx indicates dispersion, whilst a negative value indicates aggregation. The larger the absolute value of PADx, the stronger the corresponding effects. Variation in PADx in the treated residues is presented in Fig. 3. For FW treatments, the absolute values of $PAD_{0.25}$ were 3.71%, 3.80%, 13.2%, 5.68%, 12.52%, and 10.02% when the concentration of $CaCl_2$ solution was 10, 20, 50, 80, 100, and 200 mmol/L, respectively. This indicated that $CaCl_2$ had a significant protective effect on >0.25 mm residue aggregates. Compared to $PAD_{0.25}$, the absolute value of $PAD_{0.05}$ was smaller, which indicated that $CaCl_2$ had a stronger aggregation effect on >0.25 mm aggregates. The values of $PAD_{0.25}$ and $PAD_{0.05}$ for NaCl treated residues were positive, and significantly higher than those following $CaCl_2$ treatment. This demonstrates that NaCl had an clear dispersive effect on residue aggregates. For FW, SW or WS treatments, the absolute values of $PAD_{0.25}$ and $PAD_{0.05}$ balance with the concentrations of NaCl or $CaCl_2$ ranging from 50 mmol/L to 80 mmol/L, but then decrease gradually. Zhu et al., (2016) observed that with the removal of salinity, clay-sized aggregates increased and microaggregate stability decreased in bauxite residues. Soluble salts may exist as a solid state and bind fine particles to improve aggregation (Bronick and Lal, 2005). Amézketa (1999), stated that low electrolyte concentrations and high SAR (Sodium Adsorption Ratio) values produced clay dispersion and swelling. With the increase in soluble ions, electrolyte concentrations of the residue solutions increased, which may have resulted in particle aggregation. Furthermore, Na^+ addition increased the SAR values which may have led to a loss in aggregate structure. Therefore, following NaCl or $CaCl_2$ additions, the values of $PAD_{0.25}$ and $PAD_{0.05}$ varied in volatility.

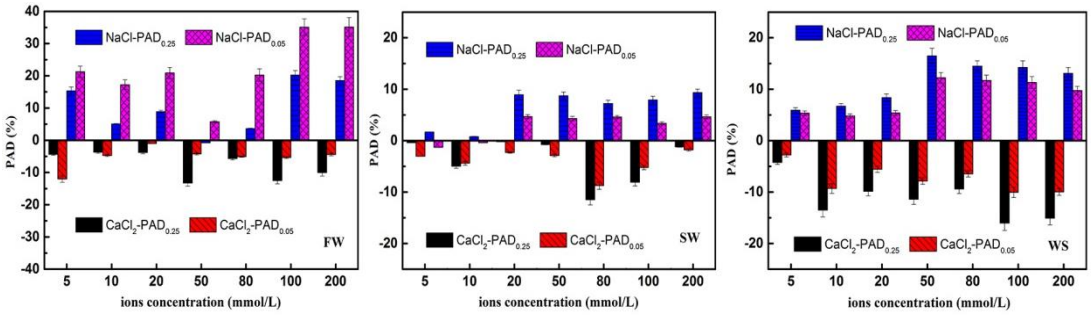

Fig. 3 Effect of Ca^{2+}/Na^{+} on the percentage of aggregate destruction of bauxite residues. a) FW test; b) SW test; c) WS test.

3.2 Effect of Ca^{2+}/Na^{+} on aggregate surface properties

Variations in pH of bauxite residue microaggregates (<0.05 mm) following the different electrolyte treatments are presented in Table 1. pH declined gradually with less than 20 mmol/L Ca^{2+}, but decreased sharply to approximately 8 when Ca^{2+} exceeded 50 mmol/L. Ca^{2+} may bind to alkaline anions (e.g. CO_3^{2-}) in the residues to form insoluble calcium-containing minerals to decrease the pH of the solution. With addition of Na^{+}, pH did not change. pH varied the composition of cations in solution, which may affect electrochemical properties (e.g. charge density, surface potential, surface charge) of the surface of residue aggregates. Calcium reduced the OH^{-} concentration and the negative surface charge on residue particles, which may reduce particle repulsion and improve aggregation.

Table. 1 Effect of Ca^{2+}/Na^{+} on pH of bauxite residue

pH	Electrolyte concentration (mmol/L)							
	0	5	10	20	50	80	100	200
Na^{+}	11.18±0.21	10.89±0.13	10.94±0.12	10.69±0.22	10.60±0.30	10.66±0.20	10.64±0.19	10.67±0.22
Ca^{2+}	11.13±0.31	10.82±0.15	10.65±0.40	10.16±0.21	8.21±0.32	7.64±0.13	7.72±0.34	7.79±0.10

The composition of ions significantly varied soil surface properties including electric field intensity, surface potential, and specific surface area of aggregates. Effects of Ca^{2+}/Na^{+} on surface properties of <0.05 mm residue aggregates are presented in Fig. 4. With an increase in electrolyte concentration, both electric field intensity and surface potential decreased. Parsons et al., (2011) observed that the increased electrolyte concentration had a strong compression effect, reducing the electric double layer of colloidal particles, which may improve the counter ions to shield the surface charge and decrease the surface potential of microaggregates. Ca^{2+} is a divalent ion, which may produce a stronger compression effect on the electric double layer than that of Na^{+} (Pashley, 1981). Therefore, the surface potential of microaggregates following Ca^{2+} addition was smaller. With an increase in Ca^{2+} concentration, the specific surface area of microaggregates decreased from 6.12 m^2/g to 0.68 m^2/g. Furthermore, the specific surface area increased to 13.3 m^2/g following Na^{+} addition. This was because flocculation or dispersion of particles determined the changes of specific surface area. Ca^{2+} promoted the stability of microaggregates, whilst Na^{+} resulted in particle dispersion

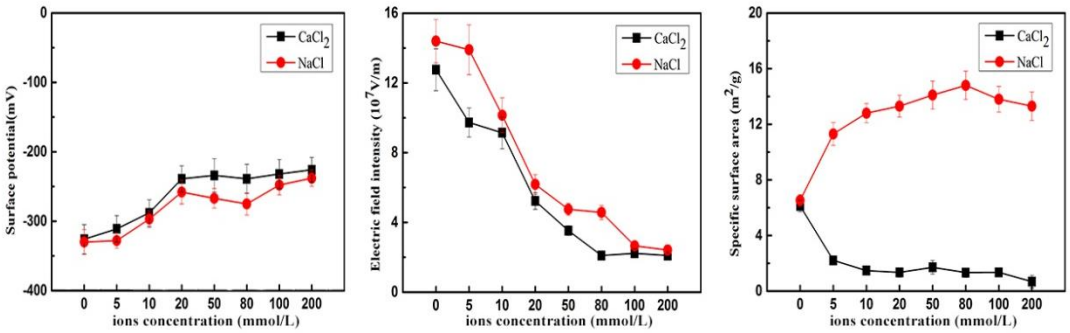

Fig.4 Effect of Ca^{2+}/Na^+ on surface properties of <0.05 mm residue aggregates.

3.3 Effect of Ca^{2+}/Na^+ on pedogenic aggregate behavior

Aggregate behavior results are depicted as either continuous surfaces plots which portray changes in the overall size distribution over time (Fig. 5A-C), or in the proportion of individual size fractions (Fig. 5a-c). This represents a detailed view of aggregate disintegration and hydrodynamic behavior in deionized water and other solution electrolytes. For the different treatments, the fastest disintegration rate in the first 20 minutes decreased as follows: Na>DI>Ca (Fig. 5A-C). PSD of the three samples varied in the first 60 minutes and then approached a stable state. Variation in PSD in the salt solutions was different, which indicated that residue aggregates exhibited diverse disintegration and hydrodynamic behaviors under the effects of different ions.

For NaCl treated residues, the initial PSD peak disintegrated following a 30-minute circulation, but then stabilized and persisted during the remaining circulation time (Fig. 5A). During circulation, a peak of 20-50 μm appeared, revealing that fractions >250 μm disintegrated into 20-50 μm smaller particles. For the control samples, the initial flat peak of PSD occurred in the range of 2-250 μm after a 20-min circulation period (Fig. 5B). This indicated that large size aggregates may disintegrate into microaggregates in the presence of Na^+. For $CaCl_2$ treated residues, the initial peak of PSD collapsed at a circulation time of 40 minutes, and the peak height remained at approximately 1.5% at the end of the circulation period (Fig. 5C).

Tisdall and Oades, (1982) proposed a hierarchical model according to the soil aggregate formation process; principally, primary particles (<20 μm) and the cements bond together to form microaggregates (20-250 μm), and thereby form larger aggregates (>250μm). Variations between the size fractions (>250 μm, 100-250 μm, 20-100 μm and <20 μm) over time and the aggregate disintegration model by the first-order rate equation are presented in Fig. 2a-c. In most cases, the first-order rate equation can fit the trend of PSD, which provided details of aggregation behavior that could not be clearly expressed in the three-dimensional surface map. The first-order rate equation parameters for different partial particles in different treatments are presented in Table 2. After circulation for 180-minutes, variations in C_1 and C_2 values revealed that Ca^{2+} addition increased the water-stable aggregate content, whilst Na^+ promoted dispersion of residue aggregates. The >250 μm aggregate fraction mainly included macro-aggregates, medium to coarse sand grains, and larger coarse mineral fragments. This fraction dispersed rapidly, with at least half of the decline occurring in the first 20 minutes and almost all of it within approximately 60 minutes (Fig. 5a-c). The 100-250 μm aggregate fraction included medium sand grains and large size micro-aggregates. Following the first 10 minutes of circulation, the 100-250 μm aggregate fraction fell

sharply, but then slowly declined. This reflected that the 100-250 μm aggregates were rapidly disaggregated into <100 μm aggregates, followed by slow disintegration of the latter into primary mineral particles and smaller microaggregates. The short-term fluctuation of >250 μm and 100-250 μm aggregates was probably due to a relatively small number of sand-sized particles, and aggregates or coarse organic fractions that could not be acquired homogeneously by the particle size analyzer pump, thereby producing substantial fluctuations. Furthermore, the 20-100 μm aggregates varied monotonically, representing a slightly decrease in microaggregates with small particle size with long-term circulation. This indicates that >100 μm fractions disaggregate into finer particles under the action of hydraulic power. In contrast, trends for <20 μm aggregates increased rapidly with almost all within 60 minutes, clearly reflecting disintegration of microaggregates. The <20 μm fractions included clay-size particles, humic materials and other cements. The results demonstrated that residue aggregates with a large size mainly disaggregated into <20 μm fractions according to the trends of these fractions with circulation time.

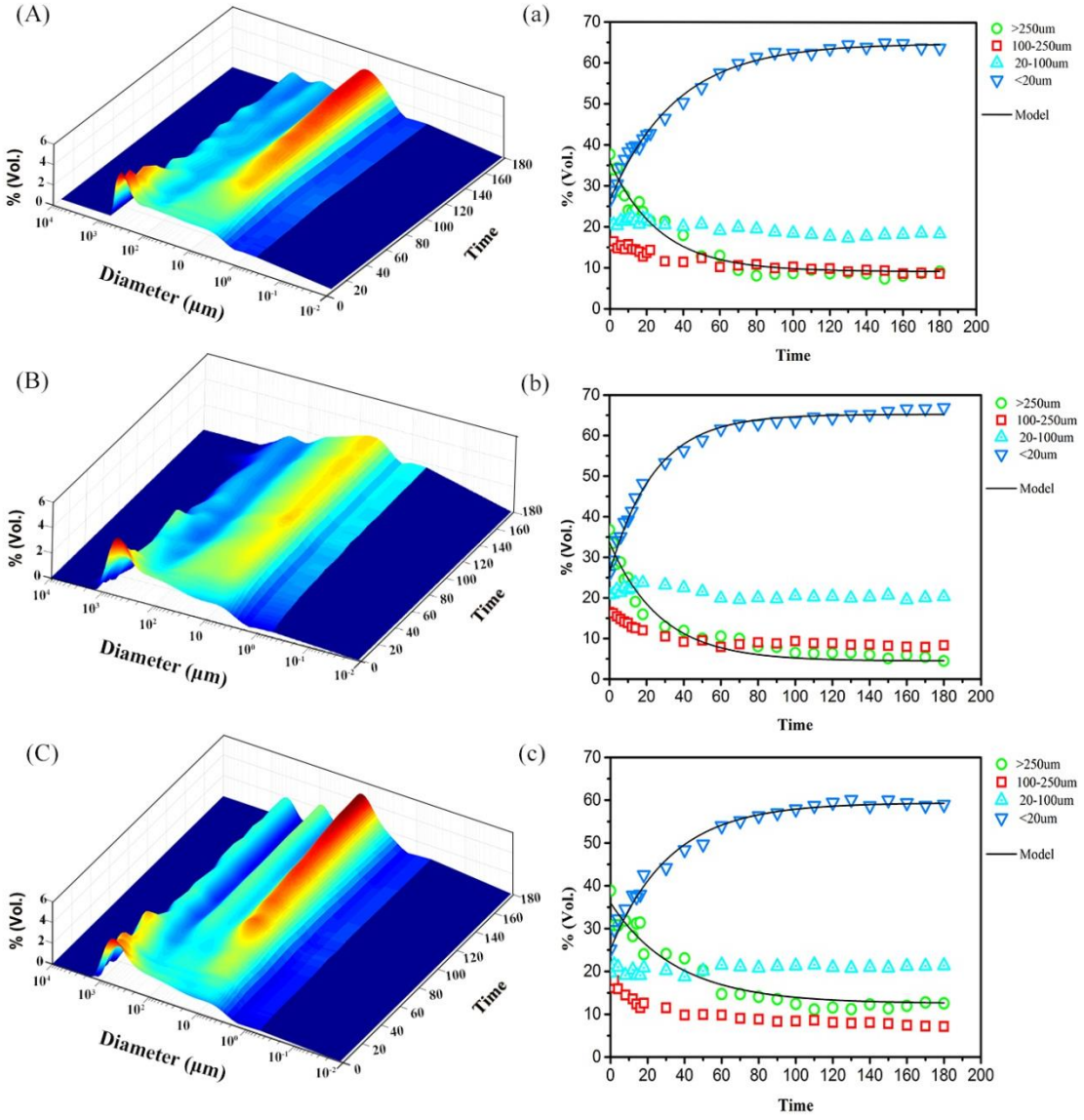

Fig.5 Surfaces representing change in particle size distribution with time, for bauxite residue after Ca^{2+}/Na^{+} treatment. Height of surface represents volumetric percentage in each particle diameter class, as it changes over time from 0 to 180 min of circulation.

Variations for multiple size fractions over the course of the experiment, lines represent first-order models fit to decrease of >250 μm or increase of <20 μm fraction. A & a) control, B & b), Na^+ and C & c) Ca^{2+}.

The results showed that the method described by Mason et al., (2011) and Kasmerchak et al. (2018) could evaluate aggregate behavior of bauxite residue following Ca^{2+} or Na^+ treatments. Three-Dimensional surfaces and variations of specific particles intuitively reflect aggregate behavior during 180 minutes of circulation. Zeng et al., (2011) investigated the effects of monovalent and divalent salt-based ions on soil aggregation, and observed that the >0.25 mm macroaggregates contained higher contents of salt ions, especially for multivalent metal ions than those in microaggregates. The increase in monovalent ions and the leaching of divalent ions may lead to the dispersion of aggregates and the deterioration of soil quality. All treatments revealed that the majority of >0.25 mm aggregates disintegrated and the small sized aggregates persisted after circulation. The presence of water molecules swelling the mineral crystal lattice, may have stimulated clay dispersion (Pashley and Israelachvili, 1984). Furthermore, residue aggregates disintegrated more rapidly in the presence of Na^+, whilst Ca^{2+} in solution could form ion bridges in the electric double layer and reduce the expansion of water molecules.

Table 2. Parameters used to model aggregate breakdown as a first-order process

treatment	A_1	K_1	C_1	R_1^2	A_2	K_2	C_2	R_2^2	a	b	c
control	26.6140	0.0371	9.2105	0.9669	38.2703	0.0278	26.5515	0.9922	25.6455	37.2222	0.6890
Na^+	29.2771	0.0365	4.4581	0.9630	39.2036	0.0418	26.0496	0.9938	28.2280	37.6005	0.7507
Ca^{2+}	23.4984	0.0280	12.5148	0.9406	34.1733	0.0313	25.2214	0.9842	22.8493	33.1199	0.6899

* $a= A_1*\exp(-k_1)$ $b=A_2*\exp(-k_2)$ $c=a/b$

3.4 Effect of Ca^{2+}/Na^+ on aggregate micro-morphology

The presence of Ca or Na changed the surface properties, affected aggregate behavior, and varied aggregate size distribution of bauxite residue. SEM-EDS analysis was used to determine changes in micro-morphology and elemental distribution of <0.05 mm residue aggregates. SEM images of the three treatments (Na^+, DI, and Ca^{2+}) are presented in Fig. 6. Scanning electron microscope imaging of control samples revealed that 0.2-1 μm particles were the major fraction present. Control residue microaggregates had sheet- or prismatic-like structures and there were relatively few fine fragments. With addition of NaCl, microaggregates sizes became smaller and the fine fragments increased. The major fractions of Ca-treated microaggregates were 0.5-1 μm particles and their structure was converted from a sheet-like to prismatic-like form. The variation in residue micro-morphology directly reflected the input of Ca^{2+}, by revealing that it could improve aggregate structure and enhance aggregate stability of residues. Similarly, using a combination methods including SEM-EDS and synchrotron-based X-ray micro-computed tomography, gypsum has been shown to improve particle size of residue aggregates, enhancing the number of large pore spaces (Xue et al., 2019). Multivalent ions such as Ca^{2+} may bind clay particles and organic matter to enhance particle agglomeration, or Ca^{2+} may exist as carbonate precipitates to form carbonate coatings and bind mineral particles together to inhibit clay dispersion (Jiang et al., 2012). Kong et al., (2017) investigated acid transformation of bauxite residue, they found that gypsum addition promoted the leaching of sodium ions and accelerated the 0.2-1 μm particle fraction in 2-5 μm aggregates due to calcium's positive effect.

According to EDS analysis, Na, Ca, Al and Fe on the surfaces of residue aggregates were the major

chemical elements. The mass fractions of Na, Ca, Al and Fe on the surfaces accounted for 4.45%, 7.33%, 27.47%, and 25.49%, respectively. Addition of $CaCl_2$ significantly accumulated Ca whilst reducing Na. This indicated that Ca^{2+} could replace exchangeable Na^{+} on the surface of the particles and the extra Na^{+} would be leached out in solution. Ca^{2+} on the aggregate surface may then improve aggregate structure and micro- morphology of the residues.

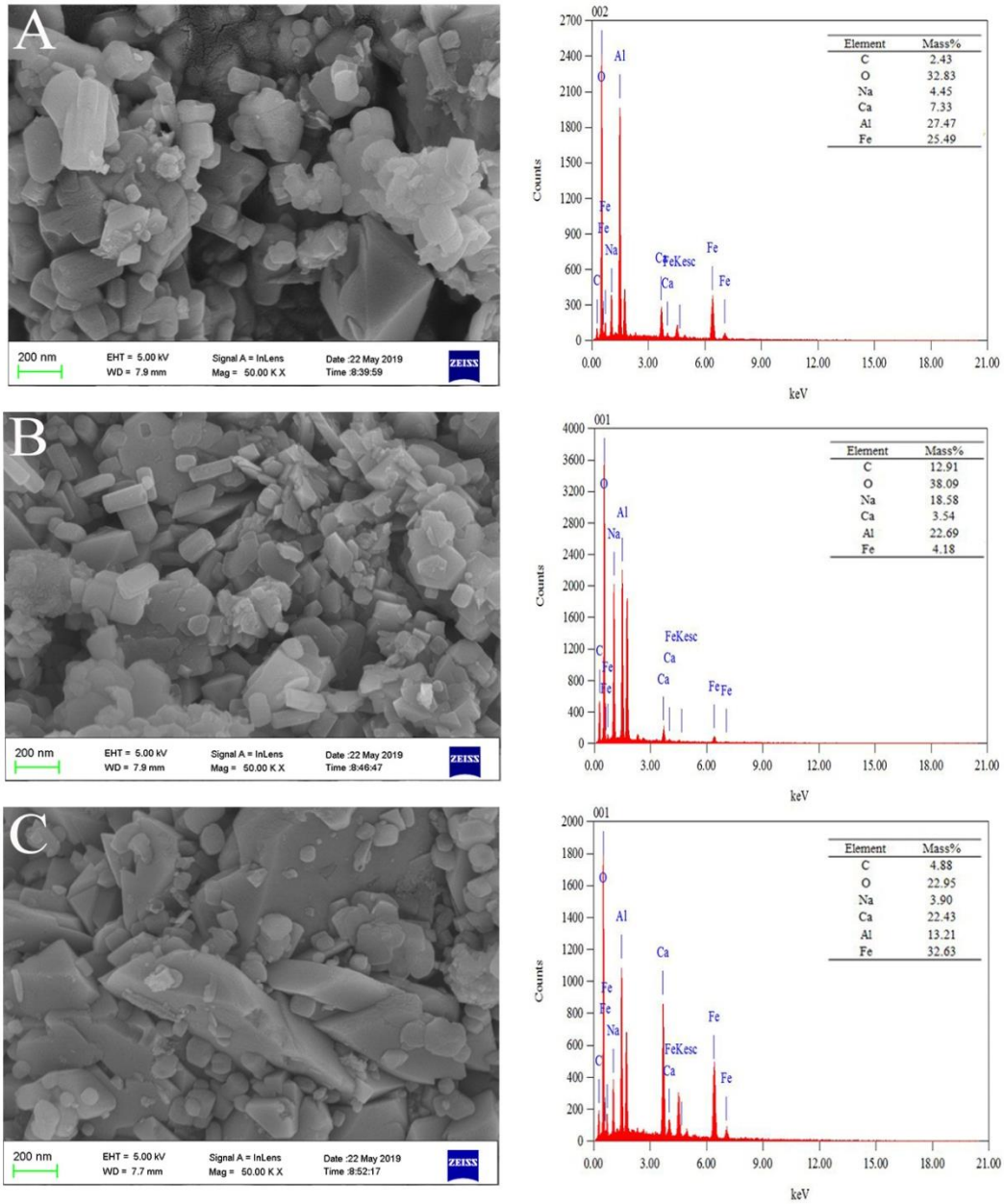

Fig.6 Morphological structure and energy-dispersive x-ray analysis spectrums of <0.05 mm residue aggregates. A, Control; B, Na^{+} (50 mmol/L); C, Ca^{2+} (50 mmol/L)

4. Conclusion

Aggregate behavior and stability of bauxite residue as affected by Ca^{2+}/Na^{+} additions were evaluated in this study. With increasing Ca^{2+} content, mean weight diameter (MWD) increased due to the

flocculation of silt-sized microaggregates. Water-stable aggregates >0.25 mm disintegrated significantly following Na^+ addition. Surface potential and electric field intensity of residue microaggregates gradually decreased with increasing electrolyte concentration. Furthermore, surface potential and electric field intensity in the Ca^{2+} system was lower than that in the Na^+ system, which may contribute to aggregate flocculation. Laser diffraction analysis allowed for continuous monitoring of aggregate disintegration during 180 minutes of circulation in solutions. Aggregate size, structure and elemental distribution changed significantly following Ca^{2+}/Na^+ treatments. These findings provide a new approach to determine the pedogenic behavior of aggregates, whilst revealing the effects of major salt ions on aggregate stability and micromorphology. Future research should focus on application of this technique in order to reveal pedogenic aggregate behavior at bauxite residue disposal areas following ameliorant and microorganism applications.

Acknowledgements

This research received funding from the National Natural Science Foundation of China (Grant No. 41701587, 41877511), and the Fundamental Research Funds for the Central Universities of Central South University (No. 202045010).

References:

Almajmaie, A. , Hardie, M. , Acuna, T. , Birch, C., 2017. Evaluation of methods for determining soil aggregate stability. Soil Till. Res. 167, 39-45..

E. Amézketa., 1999. Soil aggregate stability: a review. J. Sustain Agr. 14(2),83-151.

Bernard Barthès, Roose, E., 2002. Aggregate stability as an indicator of soil susceptibility to runoff and erosion; validation at several levels. Catena 47(2), 0-149.

Bronick, C. J. , Lal, R., 2005. Soil structure and management: a review. Geoderma 124(1-2), 0-22.

Burke, I. T. , Peacock, C. L. , Lockwood, C. L. , Stewart, D. I. , Mortimer, R. J. G. , & Ward, M. B. , et al., 2013. Behavior of aluminum, arsenic, and vanadium during the neutralization of red mud leachate by hcl, gypsum, or seawater. Environ. Sci. Technol. 47(12), 130605152436005.

Cui, H., Ou, Y., Wang, L., Wu, H., Yan, B., Li, Y., 2019. Distribution and release of phosphorus fractions associated with soil aggregate structure in restored wetlands. chemosphere.

Curtin, D., Steppuhn, H., Selles, F., Mermut, A.R., 1995. Sodicity in irrigated soils in Saskatchewan: Chemistry and structural stability. Can. J. Soil Sci. 75, 177-185.

Field, D. J. , Minasny, B., 1999. A description of aggregate liberation and dispersion in a horizons of australian vertisols by ultrasonic agitation. Geofis. Int. 91(1), 11–26.

Field, D.J., Minasny, B., Gaggin, M., 2006. Modelling aggregate liberation and dispersion of three soil types exposed to ultrasonic agitation. Soil. Res. 44, 497.

Graefe, M., Power, G., Klauber, C., 2012. ChemInform Abstract: Bauxite Residue Issues: Part 3. Alkalinity and Associated Chemistry. Cheminform 43, Graefe, M. , Power, G. , & Klauber, C., 2012. Cheminform abstract: bauxite residue issues: part 3. alkalinity and associated chemistry. Cheminform, 43(39).

Guber, A., K., Pachepsky, Ya., A., Levkovsky, E., V., 2005. Fractal mass-size scaling of wetting soil

352 aggregates. Ecol. Model. 182, 317-322.
353 Hu, F., Xu, C., Li, H., Li, S., Yu, Z., 2015. Particles interaction forces and their effects on soil aggregates
354 breakdown. Soil Till. Res. 147, 1-9.
355 Jiang, C.L., Séquaris, J.M., Vereecken, H., Klumpp, E., 2012. Effects of inorganic and organic anions
356 on the stability of illite and quartz soil colloids in Na-, Ca- and mixed Na – Ca systems. Colloid
357 Surface A. 415, 134-141.
358 Kasmerchak, C.S., Mason, J.A., Mengyu, L., 2018. Laser diffraction analysis of aggregate stability and
359 disintegration in forest and grassland soils of northern Minnesota, usa. Geoderma,
360 S0016706117320384-.
361 Kong, X., Li, M., Xue, S., Hartley, W., Chen, C., Wu, C., Li, X., Li, Y., 2017. Acid transformation of
362 bauxite residue: Conversion of its alkaline characteristics. J. Hazard Mater. 324, 382-390.
363 Le Bissonnais, Y., 1996. Aggregate stability and assessment of soil crustability and erodibility: i. theory
364 and methodology. Eur. J. Soil. Sci. 47(4), 425-437.
365 Le Bissonnais, Y., 2016. Aggregate stability and assessment of soil crustability and erodibility: I. Theory
366 and methodology. Eur. J. Soil Sci. 67, 11-21.
367 Li, H., Hou, J., Liu, X., Li, R., Zhu, H., Wu, L., 2011. Combined Determination of Specific Surface Area
368 and Surface Charge Properties of Charged Particles from a Single Experiment. Soil Sci. Soc. Am.
369 J. 75(6), 2128.
370 Li, S., Li, H., Xu, C.Y., Huang, X.R., Xie, D.T., Ni, J.P., 2013. Particle Interaction Forces Induce Soil
371 Particle Transport during Rainfall. Soil Sci. Soc. Am. J. 77, 1563.
372 Mason, J.A., Greene, R.S.B., Joeckel, R.M., 2011. Laser diffraction analysis of the disintegration of
373 aeolian sedimentary aggregates in water. Catena 87(1), 107-118.
374 Mbagwu, J.S.C., Auerswald, K., 1999. Relationship of percolation stability of soil aggregates to land use,
375 selected properties, structural indices and simulated rainfall erosion. Soil Till. Res. 50, 197-206.
376 Olis, A.C., 1989. Chemistry of Clays and Clay Minerals. soil sci. 147, 309.
377 Papadopoulos, A., Bird, N.R.A., Whitmore, A.P., Mooney, S.J., 2009. Investigating the effects of organic
378 and conventional management on soil aggregate stability using X-ray computed tomography. Eur.
379 J. Soil Sci. 60(3), 360-368.
380 Parsons, D.F., Mathias, B.M., Pierandrea, L.N., Ninham, B.W., 2011. Hofmeister effects: interplay of
381 hydration, nonelectrostatic potentials, and ion size. Phys. Chem. Chem. Phys. 13(27), 12352.
382 Pashley, R.M., 1981. DLVO and hydration forces between mica surfaces in Li + , Na + , K + , and Cs +
383 electrolyte solutions: A correlation of double-layer and hydration forces with surface cation
384 exchange properties. J. Colloid interf. Sci. 83, 531-546.
385 Pashley, R.M., Israelachvili, J.N., 1984. Molecular layering of water in thin films between mica surfaces
386 and its relation to hydration forces. J. Colloid interf. Sci. 101, 511-523.
387 Santini, T.C., Kerr, J.L., Warren, L.A., 2015. Microbially-driven strategies for bioremediation of bauxite
388 residue. J. Hazard Mater. 293, 131-157.
389 Santos, A.P.D., Yan, L., 2011. Ion specificity and the theory of stability of colloidal suspensions. Phys.
390 Rev. Lett. 106(16), 167801.
391 Shainberg, I., Singer, M.J., 2011. Soil Response to Saline and Sodic Conditions. Agricultural Salinity
392 Assessment and Management, 139-167.
393 Tang, J., Mo, Y., Zhang, J., Zhang, R., 2011. Influence of biological aggregating agents associated with

microbial population on soil aggregate stability. Appl. Soil Ecol. 47, 153-159.
Tisdall, J.M., Oades, J.M., 1982. Organic matter and water-stable aggregates in soils. Eur. j. soil sci. 33, 141-163.
Xu, G., Ding, X., Kuruppu, M., Zhou, W., Biswas, W., 2018. Research and application of non-traditional chemical stabilizers on bauxite residue (red sand) dust control, a review. Sci. Total Environ. 616-617.
Xue, S., Wang, Q., Tian, T., Ye, Y., Zhang, Y., Zhu, F., 2019. Regional-scale investigation of salt ions distribution characteristics in bauxite residue: A case study in a disposal area. J. Cent. South Univ. 26, 422-429.
Xue, S., Wu, Y., Li, Y., Kong, X., Zhu, F., William, H., Li, X., Ye, Y., 2019. Industrial wastes applications for alkalinity regulation in bauxite residue: A comprehensive review. J. Cent. South Univ. 26, 268-288.
Xue, S., Ye, Y., Zhu, F., Wang, Q., Jiang, J., Hartley, W., 2019. Changes in distribution and microstructure of bauxite residue aggregates following amendments addition. J. Environ. Sci-China. 78, 276-286.
Xue, S., Zhu, F., Kong, X., Wu, C., Huang, L., Huang, N., Hartley, W., 2016. A review of the characterization and revegetation of bauxite residues (Red mud). Environ. Sci. Pollut. R. 23, 1120-1132.
Yang, C., Liu, N., Zhang, Y., 2019. Soil aggregates regulate the impact of soil bacterial and fungal communities on soil respiration. Geoderma 337, 444-452.
You, F., Dalal, R., Huang, L., 2018. Initiation of soil formation in weathered sulfidic Cu-Pb-Zn tailings under subtropical and semi-arid climatic conditions. Chemosphere 204, 318-326.
You, F., Zhang, L., Ye, J., Huang, L., 2019. Microbial decomposition of biomass residues mitigated hydrogeochemical dynamics in strongly alkaline bauxite residues. Sci. Total Environ. 663, 216-226.
Zhu, F., Hou, J., Xue, S., Wu, C., Wang, Q., Hartley, W., 2017. Vermicompost and Gypsum Amendments Improve Aggregate Formation in Bauxite Residue. Land Degrad. Dev. 28, 2109-2120.
Zhu, F., Huang, N., Xue, S., Hartley, W., Li, Y., Zou, Q., 2016. Effects of binding materials on microaggregate size distribution in bauxite residues. Environ. Sci. Pollut. R. 23, 1-9.
Zeng L S, Gao Y, Li J L., 2011. Relationship between the composition of exchangeable base cation in soil aggregate and soil glomeration of greenhouse in Shouguang. J. Soil Water Conserv-China. 25(5): 224-228.